RSC Advances

ROYAL SOCIETY OF CHEMISTRY

www.rsc.org/advances

RSC Advances

PAPER

Novel (*E*)-1-(pyrrole-2-yl)-3-(aryl)-2-(propen-1-one) derivatives as efficient singlet oxygen quenchers: Kinetics and quantum chemical calculations

Received 00th July 2015,
Accepted 00th XXX 2015

DOI: 10.1039/x0xx00000x

www.rsc.org/

Carlos E. Diaz-Uribe,*[a] William Vallejo,[a] Wilmar Castellar,[a] Jorge Trilleras,[b] Stephanie Ortiz,[b] Angela Rodriguez-Serrano,[c] Ximena Zarate[d] and Jairo Quiroga[e]

Chalcones constitute an important group of natural and synthetic products that have been screened due to their wide range of pharmacological applications. Herein, we studied the antioxidant activity of five newly synthetized (*E*)-1-(pyrrole-2-yl)-3-(aryl)-2-(propen-1-one) (PAPs) derivatives against singlet oxygen ($^1O_2$). The differences among the compounds are related to the aryl substitution in the *p*-position where: **3a** = C_6H_5, **3b** = 4-$H_3COC_6H_4$, **3c** = 4-FC_6H_4, **3d** = 4-ClC_6H_4, **3e** = 4-BrC_6H_4. The PAPs were synthesized by Claisen–Schmidt condensation reaction between 2-acetylpyrrole and aromatic aldehydes under ultrasonic irradiation (yields between 79–86%) and were characterized by IR, mass spectrometry, NMR and quantum chemical calculations. The total singlet oxygen quenching rate constants (k_Q) by the PAPs were measured spectrophotometrically in ethanol at 25 °C and determined by using the Stern-Volmer model. As the character of the EWGs is increased from **3a** to **3e**, the k_Q diminishes smoothly. The best quencher is found to be the **3a** compound (where the aryl group is unsubstituted) with a k_Q = 5.71 (±0.21) x10^7 M^{-1} s^{-1}, which is similar to those for other antioxidants e.g. flavonoids. These results suggest these compounds as efficient quenchers of singlet oxygen and their potential aplicability in biological systems.

1. Introduction

The lowest excited electronic state of molecular oxygen, commonly known as singlet oxygen ($^1O_2(a^1\Delta_g)$), is a reactive oxygen species of special interest in chemical and medicinal research over the years. Its unique reactivity in a number of photochemical processes in a variety of systems[1-3] including e. g. lipids, sterols, proteins, DNA, and RNA[4-5] results in the degradation of biological systems and cell death. These events have been associated to different pathologies such as pigmentation, cataract, skin aging, and cancer.[6-8] Several antioxidants are known to quench singlet oxygen, both by physical and chemical mechanisms, the protective effects of the natural antioxidant constituents of fruit and vegetables have been attributed to the carotenoids, vitamins C, E and the flavonoids.[9] Nevertheless, a recent study demonstrates that intracellular singlet oxygen is not efficiently deactivated by β-carotene (*in vivo*).[10]

Antioxidant properties of flavonoids have been extensively studied *in vitro* due to their nutritional and medical relevance.[11] These compounds may function as quenchers of singlet oxygen (Eq. 1), leading to mechanisms that can be merely collisional (physical quenching, k_q), with regeneration of ground state triplet oxygen, or the interaction can result in a chemical reaction (reactive quenching, k_r), where the compounds are oxidized. When more than one process contributes to the total rate (k_Q), they need to be considered together ($k_Q = k_q + k_r$)

$$^1O_2 + \text{Flavonoid} \xrightarrow{k_Q} \text{Physical Quenching } (k_q) + \text{Chemical Reaction } (k_r) \quad (1)$$

The singlet oxygen quenching rates k_Q by flavonoids have been reported.[12-13] The physical quenching mechanism of certain electron-rich systems is known to be charge transfer. The formation of an exciplex takes place with subsequent decay to ground-state compounds and is related to the oxidation potential. Molecules with low oxidation potentials (*Eox* ≤ 1.9 V vs SCE) are efficient quenchers of $^1O_2$. In flavonoids the efficiency of the physical quenching (k_q) is mainly controlled by the presence of a catechol moiety on ring B, whereas the structure of ring C (particularly the presence of a hydroxyl group activating the 2,3-double bond) is the main factor determining the efficiency of the chemical reactivity (k_r) of flavonoids with $^1O_2$. The total reactivity scale (k_Q) is dominated by k_q, which is in general higher than k_r.[14]

[a] Grupo de Investigación en Fotoquímica y Fotobiología. Universidad del Atlántico. Kilómetro 7 Vía Puerto Colombia, Barranquilla, Colombia. e-mail: carlosdiaz@mail.uniatlantico.edu.co
[b] Grupo de Investigación en Compuestos Heterocíclicos. Universidad del Atlántico. Kilómetro 7 Vía Puerto Colombia, Barranquilla, Colombia.
[c] Grupo de Fotodinámica Molecular, Universidad de los Andes, Carrera 1 No. 18A - 10, Bogotá, Colombia. e-mail: as.rodriguez@uniandes.edu.co
[d] Instituto de Ciencias Químicas Aplicadas, Facultad de Ingeniería, Universidad Autónoma de Chile, Av. Pedro de Valdivia 641, Santiago, Chile.
[e] Grupo de Investigación de Compuestos Heterocíclicos, Universidad del Valle, A. A. 25360, Cali, Colombia.

†Electronic Supplementary Information (ESI) available: Cartesian coordinates (and geometries) of the ground and first triplet states computed by quantum chemical calculations as well as the IR and NMR experimental spectra are presented. See DOI: 10.1039/x0xx00000x

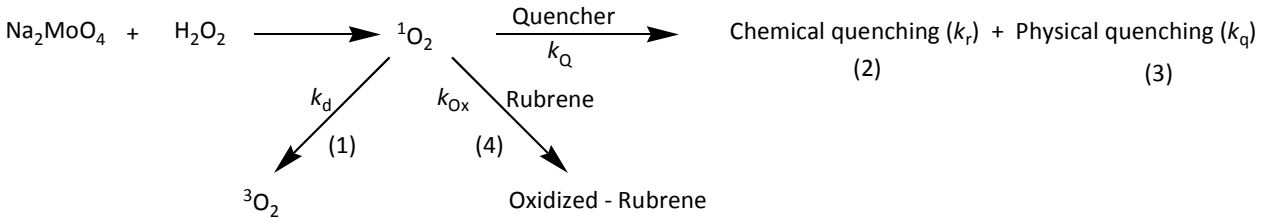

Scheme 1 Singlet oxygen oxidation of rubrene induced by $NaMoO_4$ and hydrogen peroxide under dark condition.

Nowadays, there is a great interest in the pharmacological potential of chalcones as they are precursors of flavones, isoflavones, aurones and anthocyanins which are regarded as cyclic chalcones, and their closely related physiological and medical relevancies.[15-16] This family of molecules constitutes an important group of natural and synthetic products that have been screened for their wide range of pharmacological activities as antibacterial, anti-tumor, anti-inflammatory, antifungal and antioxidant agents.[17-18]

Chalcones are 1,3-diphenyl-2-propene-1-ones, where two aromatic rings are linked by a three carbon α,β-unsaturated carbonyl system. These structures can be easily synthesized by the Claisen–Schmidt condensation, as used in this work, which involves cross aldol condensation of appropriate aldehydes and ketones by base catalysed or acid catalysed reactions followed by dehydration. Because of their pharmaceutical importance, in the present investigation we have studied the antioxidant activity of the newly synthetized (*E*)-1-(1H-pyrrol-2-yl)-3-arylprop-2-en-1-one derivatives **3(a–e)** (PAPs) against singlet oxygen. The compounds were characterized by FT-IR, ^{1}H-NMR, ^{13}C-NMR and MS. The overall quenching rate constants were determined by using a Stern–Volmer plot derived from the steady-state kinetics. Theoretical calculations were performed in order to get further insights on the molecular structure, electronic and reactivity properties of these new systems.

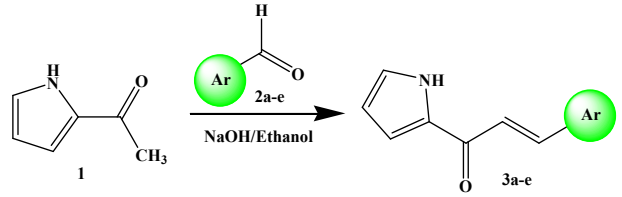

Fig. 1 Synthesis scheme of (*E*)-1-(1H-pyrrol-2-yl)-3-arylprop-2-en-1-one derivatives (PAPs). The Ar corresponds to **3a** = C_6H_5, **3b** = 4-$H_3COC_6H_4$, **3c** = 4-FC_6H_4, **3d** = 4-ClC_6H_4, **3e** = 4-BrC_6H_4.

2 Materials and Methods

2.1 Reagents and equipment

All reagents used in this work were analytical grade, the UV-Vis spectra were taken in a Hewlett-Packard 8453 spectrophotometer. FT-IR spectra (KBr) were recorded in a Bruker Tensor 27 spectrometer. Melting points were determined using a Thermo Scientific Fluke 51 II, model IA 9100 melting point apparatus and are reported uncorrected. ^{1}H NMR (400 MHz) and ^{13}C NMR (100 MHz) spectra were recorded at room temperature on a Bruker Ultra Shield 400 using $CDCl_3$ as solvent. The EIMS were run on a Shimadzu GC–MS 2010 spectrometer, which was operating at 70 eV. The IR spectra were recorded as KBr pellets on a Shimadzu FTIR-8400 instrument. The ultrasonic irradiation was performed by using a Branson ultrasonic cleaner bath, model 1510, 115v, 1.9 L with mechanical timer (60 min with continuous hold) and heater switch, 47 kHz. The aromatic aldehydes and solvents used, such as, ethanol, dichloromethane and ethyl acetate were obtained from Merck Chemical Company. 2-Acetylpyrrole was obtained from Aldrich.

2.2 General procedure for the synthesis of PAPs.

A mixture of 2-acetylpyrrole (5 mmol), appropriate aromatic aldehyde (5 mmol), NaOH (2 mmol) and ethanol (2 mL), was sonicated for 5–20 minutes in the water bath of an ultrasonic cleaner bath. The progress of the reaction was monitored by TLC using dichlorometane:ethyl acetate (9:1 v/v) as eluent. The reaction mixture was cooled in ice-water bath. The formed precipitate was filtered, washed with cool water and purified by recrystallization from ethanol to give the PAP derivatives 3(a-f) in high yields of 79–86%.

*(E)-3-phenyl-1-(1H-pyrrol-2-yl)prop-2-en-1-one (**3a**)*. IR (*v* cm^{-1}, KBr): 3237 (N-H); 1650 (C=O). NMR ^{1}H ($CDCl_3$, δ ppm): 9.98 (s, 1H, NH); 7.83 (d, *J* = 15.6 Hz, 1H, Hβ); 7.63 (m, *J* = 7.52 Hz, 2H, Ho); 7.40 (m, J = 7.27 Hz, 3H, Hm, Hp); 7.36 (d, *J* = 15.81 Hz, 1H, Hα); 7.12 (s, 1H, H5, Hetaryl); 7.09 (s, 1H, H3, Hetaryl); 6.36 (s broad, 1H, H4, Hetaryl). NMR ^{13}C ($CDCl_3$, δ ppm): 178.6 (C=O); 142.0 (Cβ); 134.7; 132.8; 129.8 (Cα); 128.6; 128.0; 125.1; 121.7; 116.1; 110.6. MS (ESI, positive scan) m/z = 197.3 (M^+).

*(E)-3-(4-methoxyphenyl)-1-(1H-pyrrol-2-yl)prop-2-en-1-one (**3b**)*. IR (*v* cm^{-1}, KBr): 3259 (N-H); 1646 (C=O). NMR ^{1}H ($CDCl_3$, δ ppm): 9.85 (s, 1H, NH); 7.79 (d, *J* = 15.6 Hz, 1H, Hβ); 7.59 (d, *J* = 8.89 Hz, 2H, Hm); 7.24 (d, *J* = 15.6 Hz, 1H, Hα); 7.09 (s, 1H, H5, Hetaryl); 7.05 (s, 1H, H3, Hetaryl); 6.93 (d, *J* = 8.78 Hz, 2H, Ho); 6.34 (s broad, 1H, H4, Hetaryl); 3.84 (s, 3H, OCH_3). NMR ^{13}C ($CDCl_3$, δ ppm): 178.7 (C=O); 161.1; 141.7 (Cβ); 132.9; 129.7; 127.5; 124.7 (Cα); 119.3; 115.6; 114.0; 110.5; 55.1. MS (ESI, positive scan) m/z = 227.9 (M^+); 160.96 (M^+- C_4H_4N).

*(E)-3-(4-fluorophenyl)-1-(1H-pyrrol-2-yl)prop-2-en-1-one (**3c**)*. IR (*v* cm^{-1}, KBr): 3266 (N-H); 1448 (C=O). NMR ^{1}H ($CDCl_3$, δ ppm): 9.62 (s, 1H, NH); 8.26 (d, J = 8.78 Hz, 2H, Hm); 7.82 (d, J = 15.8 Hz, 1H, Hβ); 7.76 (d, J = 8.78 Hz, 2H, Ho); 7.43 (d, J = 15.8 Hz, 1H, Hα); 7.15 (s, 1H, H5, Hetaryl); 7.10 (s, 1H, H3, Hetaryl); 6.38 (s broad, 1H, H4, Hetaryl). NMR ^{13}C ($CDCl_3$, δ

ppm): 188.6 (C=O); 139.2 (Cβ); 128.8; 126.1; 125.8 (Cα); 124.2; 117.0; 111.4 MS (ESI, positive scan) m/z = 215.1 (M^+).

(E)-3-(4-chlorophenyl)-1-(1H-pyrrol-2-yl)prop-2-en-1-one (***3d***). IR (ν cm^{-1}, KBr): 3273 (N-H); 1645 (C=O). NMR ^1H ($CDCl_3$, δ ppm): 11.97 (s, 1H, NH); 7.86 (d, *J* = 8.54 Hz, 2H, Hm); 7.70 (d, *J* = 15.8 Hz, 1H, Hβ); 7.62 (d, *J* = 15.5 Hz, 1H, Hα); 7.49 (d, *J* = 8.28 Hz, 2H, Ho); 7.37 (s, 1H, H5, Hetaryl); 7.16 (s, 1H, H3, Hetaryl); 6.27 (s broad, 1H, H4, Hetaryl). NMR ^{13}C ($CDCl_3$, δ ppm): 178.5 (C=O); 140.8 (Cβ); 136.0; 133.5; 133.1; 129.4; 129.1 (Cα); 125.6; 116.5; 111.1. MS (ESI, positive scan) m/z = 231.7 (M^+); 233.04 (M^+ + 2)

(E)-3-(4-bromophenyl)-1-(1H-pyrrol-2-yl)prop-2-en-1-one (***3e***). IR (ν cm^{-1}, KBr): 3270 (N-H); 1644 (C=O). NMR ^1H ($CDCl_3$, δ ppm): 10.02 (s, 1H, NH); 7.79 (d, *J* = 15.6 Hz, 1H, Hβ); 7.58 (d, *J* = 8.53 Hz, 2H, Hm); 7.53 (d, *J* = 8.28 Hz, 2H, Ho); 7.37 (d, *J* = 15.6 Hz, 1H, Hα); 7.17 (s, 1H, H5, Hetaryl); 7.12 (s, 1H, H3, Hetaryl); 6.39 (s broad, 1H, H4, Hetaryl). NMR ^{13}C ($CDCl_3$, δ ppm): 178.5 (C=O); 140.8 (Cβ); 133.9; 133.0; 132.1; 129.6; 125.7 (Cα); 124.4; 122.5; 116.6; 111.1. MS (ESI, positive scan) m/z = 275.0 (M^+); 277.1 (M^+ +2).

2.3 Determination of overall singlet oxygen quenching rate

The overall rates constants k_Q (=k_q + k_r) for the reaction of $^1O_2$ with PAPs were determined in ethanol solution at 25 °C through competition reaction method using rubrene as standard compound and analyzing the first-order rate constant (*S*) of the decay curve of rubrene. Singlet oxygen was induced from dark chemical reaction of Na_2MoO_4 and H_2O_2. The overall rate constant was determined using a Stern–Volmer plot derived from steady state kinetics (see Scheme 1). The reciprocal lifetimes were represented as a function of the PAPs concentration and the bimolecular rate constants were determined from the slope of the linear plots. The experimental errors were estimated to be <5% in the rate constants (k_Q) determination. All measurements were performed at 25 ± 0.5 °C.

Rubrene oxidation with a chemical source of singlet oxygen in microemulsion was performed to check singlet oxygen quenching activity.[19] The microemulsion was prepared at room temperature (298 K) by adding an aqueous solution of 0.2 M $Na_2MoO_4.2H_2O$ (290.4 mg in 6 mL of water) dropwise to a magnetically stirred slurry of SDS (4.7 g), 1-butanol (9.4 g), and methylene chloride (60 mL). After a few minutes, the turbid suspension was converted into a mobile and transparent liquid. Then, 2.0 x 10^{-4} mol of rubrene was introduced into a small Erlenmeyer flask plus 15 mL of microemulsion. The medium was magnetically stirred for 10 minutes and stored in darkness to prevent the autosensitized photooxidation of rubrene. After that, 50 µmol of H_2O_2 were added to the red solution and the reaction medium was stirred with a microscale magnetic bar at room temperature. The samples solutions also contained PAPs (as quenchers, 0 - 3.0x10^{-3} M). The oxidation of rubrene was monitored by visible spectroscopy at 522 nm.

2.4 Quantum chemical calculations

Geometry optimization of the electronic ground states of PAPs were performed using the B3LYP[20-21] functional and the TZVP[22] basis set as implemented in the Turbomole 6.3 program package.[23] The minima of the first triplet states (T_1) of PAPs were determined by unrestricted density functional theory (UDFT) due to triplet instabilities when using a TD-DFT gradient.[24] DFT-D3 corrections to the dispersion energy were accounted in all geometry optimizations.[25] The conductor-like screening model (COSMO, ε = 24.852) has been used for the simulation of a bulk ethanolic environment (electrostatic solvent effects).[26-28] Harmonic vibrational frequencies were computed numerically employing the SNF program.[29]

The adiabatic excitation energies of the T_1 states of PAPs were obtained from single-point energy calculations using the density functional theory / multi-reference configuration interaction (DFT/MRCI) method.[30] The main idea is to account for static electron correlation via MRCI while the dynamic electron correlation is treated by DFT. The configuration state functions (CSFs) of the MRCI expansion uses Kohn–Sham (KS) orbitals computed employing the BHLYP functional. This hybrid approximation is known to yield reliable excitation energies at a reasonable cost for medium to large size of organic chromophores and within errors around of 0.2 eV.[31-32] Here, we follow the same DFT/MRCI procedures for calculating the electronic state properties (for a C_1 point group and 10 roots for *A* representation) as in previous work.[33] The MRCI expansions were built up from the one-particle basis of the optimized Kohn–Sham orbitals with the COSMO method.

3 Results and Discussion

3.1 Synthesis and characterization of the PAPs

Conventionally, enonic derivatives are obtained via Claisen-Schmidt condensation reaction.[34] Variations in such methodology were performed, where ultrasound radiation was used during the reaction to obtain the PAPs in short time and with good yields. Since the aim was to study the antioxidant properties of the compounds, we did not evaluate the effects of other reaction parameters (temperature, catalyst and solvent). In general, for reactions of this type, the reaction rate increases with temperature.[35] The (*E*)-1-(1H-pyrrol-2-yl)-3-arylprop-2-en-1-one (PAPs) derivatives were prepared with excellent yields starting with 2-acetylpyrrole and aromatic aldehydes in the presence of NaOH (solid) in ethanol under ultrasonic irradiation at room temperature during 5–20 minutes. The yield percentage (see Table 1) of the reaction was estimated by stoichiometric analysis of the starting materials and the final weight of product obtained after purified by recrystallization with ethanol and complete drying (compared to the stoichiometric expected quantity). The structures of all the synthesized compounds were confirmed by IR, ^1H-NMR, ^{13}C-NMR and MS. The corresponding spectra for each of the compounds are provided as supporting information (SI).

The preparation of chalcones under basic conditions and using sonochemical method provides several advantages such as operational simplicity, reduction of the processing time, higher yield, safety, environment friendly protocol and to enhance the efficiency of the catalyst.[36] This is due to the rapid micromixing and the resulting faster reaction (also possibly due to the formation of local hot spots) to form the chalcone.[37-39]

Table 1. Reaction time (t_r), melting point (T_f) and % yield for compounds **3(a–e)**

Comp. 3	Ar	t_r (min.)	T_f(°C)	Yield (%)
3a	C_6H_5	10	140	86
3b	4-$H_3COC_6H_4$	5	137	86
3c	4-FC_6H_4	20	170	80
3d	4-ClC_6H_4	20	165	79
3e	4-BrC_6H_4	20	185	83

3.2 Overall rate constants (k_Q) for the quenching of $^1O_2$

Singlet oxygen decay occurs mainly via 4 routes (reactions 1 to 4, scheme 1): non-radiative decay (1), chemical quenching (2), physical quenching (3) and reaction with rubrene (4). The total quenching rate constants for the reaction of singlet oxygen with PAPs in ethanol were determined from the measured first-order decay of singlet oxygen in the absence and presence of PAPs according to Eq. 2 derived from the steady-state treatment of scheme 1 (both with same initial concentration of rubrene). The PAPs inhibited the oxidation of rubrene and its effect was concentration dependent.

$$\frac{S_0}{S_S} = 1 + \left[\frac{(k_q + k_r)}{k_d}\right][\text{PAPs}] \qquad (2)$$

Where S_0 and S_S are slopes of the first-order plots of disappearance of singlet oxygen (acceptor), rubrene, in the absence and presence of PAPs, respectively. And, k_d is the rate of deactivation of singlet oxygen in ethanol. A plot of S_0/S_S vs concentration of PAPs is shown in Fig. 2. The overall rate constants (k_Q) were calculated using the value of k_d in ethanol ($k_d = 8.3x10^4\ s^{-1}$), reported by Merkel and Kearns.[40] The k_Q values obtained for PAPs are listed in Table 2. Based on this kinetics for the oxygen quenching, the trend of the measure values upon aryl substitution show that the fastest process proceeds for the **3a** compound (*p*-unsubstituted) with a rate constant of $k_Q = 5.71 \times 10^7\ M^{-1}\ s^{-1}$. These rate constants diminishes smoothly upon *p*-substitution of the aryl group by -OCH_3, -F, -Cl and -Br (**3b-e** PAPs) maintaining the same order of magnitude. This result indicates that the PAPs can act as scavengers of singlet oxygen. It has been postulated in the literature that the bimolecular reactions of singlet oxygen (also quenching processes) may occur via a reversible and rapid formation of a charge transfer encounter complex (exciplex) that could evolve through chemical reaction pathways or singlet-singlet energy transfer.[14,41] The latter mechanism generates the triplet state of the quencher (via ISC) and the ground state of molecular oxygen. The fate in which the reaction may occur mainly via a physical or a chemical pathway is a balance between spin-orbit and electronic coupling, and entropic (diffusion) factors.

Many studies show that the substituent in the aromatic ring influence the overall rate constants values.[14,42-43] For example, k_Q increased as the number of -OH groups substituted to the aromatic skeleton (that is, the total electron-donating capacity) increases. Along, the heavy-atom contribution on rate constant k_Q has been studied, several halogenated anilines with similar oxidation potentials were used as quenchers.[44] Aniline without halogenated substituent has the higher k_Q value than the compounds with chlorine and bromine in acetonitrile, possibly due to halogens (-F, -Cl and -Br) are electron withdrawing groups (EWGs) and inefficient for electron delocalization, hence with a lower capacity to stabilize resonance structures.

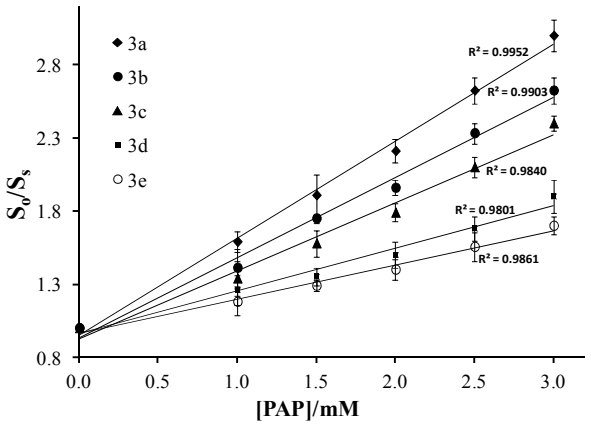

Fig. 2 Plot of S_0/S_S vs concentrations (mM) of PAPs.

Many heterocyclic compounds also act as quenchers of singlet oxygen.[45-47] The interest in obtaining this type of heterocyclic chalcone derivatives is due to their versatility as starting materials in the synthesis of a series of heterocyclic compounds.[48] However, α,β-unsaturated systems in combination with substituted aromatic rings with electron releasing groups (ERGs) and heterocyclic rings such as pyrrole (6 πe^- in a 5-membered ring) can influence the antioxidant properties of the molecule. The rate constants (k_Q) for some flavonoids are similar to PAPs: chrysin ($2.01 \times 10^7\ M^{-1}s^{-1}$),

Table 2. Overall rate constants (k_Q) for the quenching of $^1O_2$ by PAPs. DFT/MRCI adiabatic excitation energies (ΔE^{ad}) of the first triplet states (T_1) in ethanolic environment (COSMO, ε = 24.852)

Comp. 3	Ar =	k_Q ($M^{-1}s^{-1}$)	ΔE^{ad} [eV]*
3a	C_6H_5	5.71 (±0.21) x10^7	2.20(2.34)
3b	4-$H_3COC_6H_4$	4.85 (±0.10) x 10^7	2.05(2.23)
3c	4-FC_6H_4	3.87 (±0.22) x 10^7	2.24(2.39)
3d	4-ClC_6H_4	2.42 (±0.24) x 10^7	2.19(2.33)
3e	4-BrC_6H_4	1.94 (±0.18) x 10^7	2.16(2.31)

*The values in parenthesis correspond to the more unstable *anti* conformation. See details in the text, section 3.3.

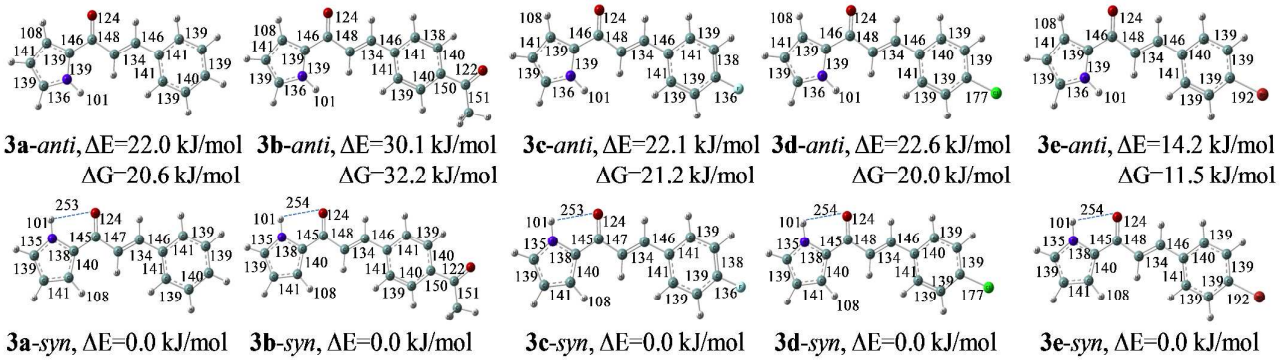

Fig. 3 Ground state minima of PAPs optimized at the B3LYP-D3/TZVP + COSMO(ε = 24.852) level of theory. Bond lengths are presented in pm. Relative energies (ΔE in kJ/mol) and Gibbs energies (ΔG in kJ/mol) of the local minima relative to the lowest energy conformer are computed using the DFT/MRCI method.

apigenin (2.84×10^7 $M^{-1}s^{-1}$), catechins (1.09×10^7 - 1.47×10^8 $M^{-1}s^{-1}$).[43] These PAPs have similar singlet oxygen quenching activity to synthetic antioxidants like *tert*-butyl-hydroxyanisol (3.37×10^7 $M^{-1}s^{-1}$) and *tert*-di-Butyl-hydroxytoluene (4.26×10^6 $M^{-1}s^{-1}$).[49] However, the quenching rate of PAPs is one to three orders of magnitude smaller than that of β-carotene (1.58×10^{10} $M^{-1}s^{-1}$) and α-tocopherol (2.06×10^8 $M^{-1}s^{-1}$), which are well known as representatives singlet oxygen quenchers.[50-51]

Most reactions of $^1O_2$ with biological targets (lipids, sterols, proteins (amino acids), DNA, and RNA occur via chemical rather than physical routes inducing cell death and mutations.[4-5] For instance, the quenching rates are 9.0×10^3 $M^{-1}s^{-1}$ for stearic acid, 1.7×10^4 $M^{-1}s^{-1}$ for oleic acid, 4.2×10^4 $M^{-1}s^{-1}$ for linoleic acid, 5.7×10^4 $M^{-1}s^{-1}$for cholesterol, and 5.1×10^5 $M^{-1}s^{-1}$ for DNA.[14] The k_Q values observed in this work are 2 to 4 orders of magnitude larger than those fatty acids and DNA. This result suggests that these compounds may contribute to the protections of the lipid peroxidation and the degradation of DNA in photosynthetic systems, by quenching $^1O_2$.

3.3 Computational studies

Herein, the results obtained by quantum chemical calculations are presented. First, the ground state geometrical properties and stability of two different conformers of PAPs are discussed. In order to open the discussion about the physical and chemical quenching of singlet oxygen by PAPs, the electronic properties computed at the adiabatic T_1 state minima and the local reactivity indexes computed at the ground state geometry are also analyzed. The cartesian coordinates of all the computed minima and the frontier molecular orbitals (MOs) computed at the T_1 states are provided in the SI.

Ground state (S_0) properties. The optimized ground state minima of PAPs at the B3LYP-D3/TZVP + COSMO(ε = 24.852) level are presented in Fig. 3. The geometries are found to be almost planar respect to the pyrrole, propenone and aryl groups; since the deviations from the planarity through these groups do not exceed 1.6° degrees. For the **3d** compound (where the *p*-substitution at the aryl group corresponds to a methoxy group) the variations can range up to 3.7°. All the calculated distances show only small variations when changing the EWG at the *p*-position by -OCH_3, -F, -Cl and -Br groups. As expected, the substitution effects are visible taking into account the differences of the calculated C-X bond lengths.

Two different molecular configurations are possible, depending on the position of the pyrrole group relative to the carbonyl oxygen (*syn* or *anti*). The *syn* configurations are found to be more stable than the *anti* conformers due to the presence of a intramolecular hydrogen bond between the carbonyl oxygen and the pyrrole proton (-C=O¨H-N-), see Fig. 3. The length of these hydrogen bonds is calculated to be of about 254 pm which is unaffected by EWGs *p*-aryl substitution. The DFT/MRCI energy difference (ΔE) between these configurations is in between 14.2 and 30.1 kJ/mol, suggesting a major population of the *syn* conformers at ambient temperature.

The T_1 ($\pi_H\pi_L$) state.* A DFT/MRCI calculation of the vertical electronic spectra of the PAPs revealed that all the T_1 states are generated by a HOMO - LUMO transition, see Fig. 4. UDFT/COSMO geometry optimizations of these states revealed true minima on the corresponding potential energy surfaces. The involved MOs are seen to be delocalized over the whole molecular structure for each of the PAPs. The HOMO and LUMO orbitals of all the compounds are very similar, a single difference in the shape of the HOMO orbital of the **3b** compound (Ar = 4-$H_3COC_6H_4$) can be seen where there is no density node at the carbonyl oxygen of the chalcone (both *syn* and *anti* configurations). This would make a difference in the energetic stability of the T_1 state.

The respective DFT/MRCI adiabatic energies (ΔE^{ad}) of the $T_1(\pi_H\pi_L^*)$ states of **3a-e** are listed in Table 2. The method places the energy of all the T_1 states above 2 eV and, as expected, again the *syn* configuration of the PAPs show a higher stability compared to the *anti* conformers (energies shown in parenthesis in Table 2). Within the *syn* series, the most stable T_1 state corresponds to the **3b**-*syn* compound (2.05 eV) while the **3c**-*syn* presents the highest energy

(2.24 eV). The adiabatic energy of the T_1 state of the PAPs tends to decrease by heavy atom effect when going from Ar = 4-FC_6H_4 to 4-BrC_6H_4.

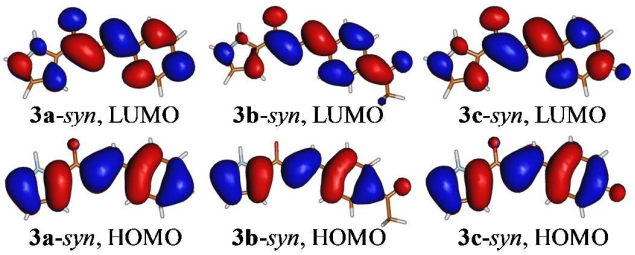

Fig. 4 BHLYP Frontier MOs of some selected PAPs calculated at the optimized B3LYP-D3/TZVP + COSMO (ε = 24.852) ground state minima.

An energy transfer process between singlet oxygen and a quencher depends on many aspects as vibronic interactions, short (*e.g.* overlap of the electron clouds) and long range (*e.g.* antenna-type dipole-dipole interactions) interactions. Nevertheless, as a general rule, there should be a very low-energy barrier for promoting a fast energy transfer. In this framework, we analyze the energy differences between singlet oxygen and the adiabatic T_1 state of PAPs.

The observed decrease on the experimental rate constants of quenching singlet oxygen from the **3a** to **3d** compounds does not correlate well with the respective trend of the adiabatic energies for the T_1 states. Moreover, being the reported energy for singlet oxygen of 0.98 eV,[52] energy transfer from singlet oxygen to the ground state of **3a-e** to produce their T_1 states (>2 eV) constitutes a endoergic process. These two facts announce that the physical quenching of singlet oxygen from PAPs is not a feasible pathway. Therefore, it is possible to suggest that the mechanism corresponds to chemical quenching.

Chemical reactivity indexes. In order to rationalize the interaction of the PAPs with singlet oxygen through a chemical quenching pathway, a set of local reactivity descriptors were computed. In the framework of the conceptual Density Functional Theory,[53] here we have analyzed the estimated chemical potential (μ), chemical hardness (η), and electrophilicity (ω).[54-57]These set of values are reported in Table 3. Moreover, the HOMO and LUMO orbitals essential for these computations are presented in Fig. 4. Accordingly we have tried to correlate the measured k_Q values with these global properties.

The μ in Eq. 3 represents the infinitesimal change of energy when electronic charge is added to a molecular system at a constant external potential of the nuclei ($v(\vec{r})$), fact closely related with its electronegativity (χ). Using a second order derivative of the chemical potential, one arrives at η (Eq. 4) and measures how the electronegativity of a system decreases when an infinitesimal amount of electronic charge is added into it.

$$\mu = \left(\frac{\partial E}{\partial N}\right)_{v(\vec{r})} = -\chi \quad (3)$$

$$\eta = \frac{1}{2}\left(\frac{\partial^2 E}{\partial N^2}\right)_{v(\vec{r})} = \frac{1}{2}\left(\frac{\partial \mu}{\partial N}\right)_{v(\vec{r})} \quad (4)$$

In numerical applications, these reactivity indexes are calculated following approximations using the Koopmans' theory and finite differences leading to Eqs. 5 and 6. Here, *I* and *A* correspond to the ionization energy and electron affinity while $E(\pi_H)$ and $E(\pi_H)$ correspond to the orbital energies of the HOMO and LUMO, respectively.

$$\mu \approx -\frac{1}{2}(I + A) \approx \frac{1}{2}(E(\pi_L) + E(\pi_H)) \quad (5)$$

$$\eta \approx \frac{1}{2}(I - A) \approx \frac{1}{2}(E(\pi_L) - E(\pi_H)) \quad (6)$$

The ω index as defined in Eq. 7 measures the propensity of a molecule to receive electronic charge from a donor. Therefore, ω is thought as a sort of "electrophilicity power".

$$\omega = \frac{\mu^2}{2\eta} \quad (3)$$

Table 3. Estimated energies for the HOMO and LUMO orbitals ($E(\pi_H)$ and $E(\pi_H)$), chemical potential (μ), chemical hardness (η), and electrophilicity (ω) calculated for the optimized B3LYP-D3/TZVP + COSMO (ε = 24.852) ground state minima of the PAPs

Comp. 3	$E(\pi_H)$/eV	$E(\pi_L)$/eV	μ/eV	η/eV	ω/eV
3a-*syn*	-6.38	-2.46	-4.42	1.96	4.99
3b-*syn*	-6.47	-2.81	-4.64	1.83	5.89
3c-*syn*	-6.37	-2.46	-4.41	1.96	4.97
3d-*syn*	-6.39	-2.53	-4.46	1.93	5.16
3e-*syn*	-6.39	-2.55	-4.47	1.92	5.19

For this analysis, we restricted the discussion to the lowest-energy *syn* conformers in the ground state. As can be seen from the data collected in Table 2, μ adopts low and similar values from compound **3a-*syn*** to **3e-*syn*** in between -4.62 to -4.41 eV. That means, these PAPs tend to react as source of electrons which enhance their antioxidant activity. While the values of μ and η diminishes as k_Q for compounds **3c-*syn*** to **3e-*syn***, ω does inversely correlate. This means that the increase of the power of the EWDs by -F, -Cl and -Br in the **3c-*syn*** to **3e-*syn*** is reasonable with respect to the impact of the global reactivity/polarization indexes indicating the presence of a charge transfer interaction with singlet oxygen in which the PAPs are the electron donors. These results confirm the nature of the quenchers. However, these trends are not well satisfied in the same manner for compounds **3a-*syn*** and **3b-*syn*** with respect the observed variations the chemical reactivity indexes for compounds **3c-*syn*** to **3e-*syn***, when addressing to the tendency of decay on k_Q. The compound **3a-*syn*** shows almost equal values than for **3c-*syn*** of the μ, η and ω indexes. While, for **3b-*syn*** these magnitudes are the smallest of the series for μ and η, and the highest for the ω index. As all the k_Q determined

experimentally are of the same order of magnitude ($\sim 10^7$ $M^{-1}s^{-1}$), in consequence, it is possible to conclude that because of this fact, the reactivity indexes display a similar description for the systems.

In order to clarify the dependency of the reactivity with singlet oxygen on the electron density among the PAPs, we had also analyzed the charge transfer properties and the condensed fukui functions. In Fig. 5, we included the wavefunctions for electrophilic (f^-) and nucleophilic (f^+) attacks. Considering that singlet oxygen may attack sites with high electron density, the double bond of PAPs would be the preferable reaction pathway for the chemical quenching. These results are consistent with the known reactivity of singlet oxygen with unsaturated fatty acids (and flavonoids) where the reaction could involve the formation of a hydroperoxide intermediate through an ene-like attack or via a [2+2] concerted-cycloaddition to form an endoperoxide. Other centers where singlet oxygen may attack can be seen in Fig. 5, where is visible that the presence of the voluminous -OCH_3 group and the heavy atoms smoothly changes the local electronic properties of the PAPs, and therefore their particular way to react. Therefore, the reactivity will depend on the interactions occurring in the encounter complex formed of PAPs with singlet oxygen where the fukui wavefunctions also show a strong amplitude at the pyrrole group.

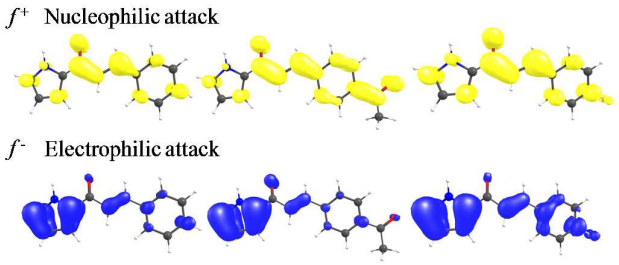

Fig. 5 Condensed fukui functions for nucleophilic (f^+) and electrophilic (f^-) attacks for compounds **3a-c**.

Although these results are not a definitive evidence on how may be the mechanism of the chemical quenching of singlet oxygen by PAPs and the corresponding correlations determined experimentally by the kinetics, they are useful for understanding their chemical behavior. In this context, it is not surprising that the reactivity indexes does not exactly correlate with the tendency of the kinetics since a variety of reaction mechanisms (as commented above, e.g., hydroperoxide and endoperoxide formation) can occur and may kinetically compete. In this case the kinetics will depend on electronic, energetic and entropic factors which is achieved analyzing the bimolecular situation. A more deep understanding of the reaction would include by a detailed exploration of the potential energy surfaces and modeling chemically active intermediates to yield the reaction products by different pathways. We are looking forward to open this discussion soon in a study under development.

4. Conclusions

In this work, we synthesized five new derivatives from (*E*)-1-(1H-pyrrol-2-yl)-3-arylprop-2-en-1-one (PAPs); compounds **3(a-e)**. The structural differences within the series is the *p*-substitution of the aryl group, where Ar = -C_6H_5, 4-$H_3COC_6H_4$, 4-FC_6H_4, 4-ClC_6H_4, 4-BrC_6H_4 respectively from **3a** to **3e**. The synthesis of the compounds was confirmed by FT-IR. ^{1}H-NMR, ^{13}C-NMR, MS. Moreover, the electronic and geometrical properties of these new chalcones were characterized by quantum chemical calculations.

Through Stern–Volmer plots and steady-state kinetical analysis, the antioxidant capacity of the PAPs against singlet oxygen has been evaluated. The large values of the rate constants demonstrated that these novel compounds could inhibit the rubrene oxidation by efficiently quenching of singlet oxygen. The best quencher is the compound **3a** (where the aryl group is unsubstituted) with a total singlet oxygen quenching rate constant (k_Q) value of 5.71 (±0.21) x10^7 M^{-1} s^{-1} in ethanolic solution. Through the heavy atom effects evaluated from compounds **3a** to **3e**, a smooth decay on k_Q values has been observed although preserving the order of magnitude. This kinetic study, therefore, suggests the applicability and evaluation of these compounds as singlet oxygen quenchers in biological systems promoting protection from oxidative damage.

Acknowledgements

The authors thank to COLCIENCIAS for financial support through contract No 0622-2013 of "*Proyectos de semilleros de investigación*" (Conv. 617/2013) and FONDECYT (11140563). A.R.-S. thanks Prof. Jörg Tatchen for helpful discussions. X.Z. thanks Fondo de Apoyo a Asistencia a Eventos Científicos Nacionales o Internacionales, Dirección de Investigación y Postgrado, Universidad Autónoma de Chile.

References

1 C. E. Diaz-Uribe, M. C. Daza, E. A. Páez-Mozo, F. Martínez, C. Guedes and E. Di Mauro, *J. Photochem. Photobiol. A*, 2013, **259**, 47-52.

2 L. A. Teixeira, M. T. Churampi, C. Marquez, L. Yokoyama and F. Da Fonseca, *Min. Eng.*, 2013, **50**, 57-63.

3 H. Yoshii, Y. Yoshii, T. Asai, T. Furukawa, S. Takaichi and Y. Fujibayashi, *Biochem. Biophys. Res. Commun.*, 2012, **417**, 640-645.

4 R. S. Ray, S. F. Mujtaba, A. Dwivedi, N. Yadav, A. Verma, H. N. Kushwaha, S. K. Amar, S. Goel and D. Chopra, *Toxicology,* 2013, **314**, 229-237.

5 Y. Wenli and Z. Yaping, *Biochim. Biophys. Acta.* 2005, **30**, 30-34.

6 X. Wen, J. Wu, F. Wang, B. Liu, C. Huang and Y. Wei, *Free Rad. Biol. Med.* 2013, **65**, 402-410.

7 M. M. Mehdi and S. I. Rizvi, *Arch. Med. Res.*, 2013, **44**, 136-141.

8 E. Bigot, r. Bataille, T. Patrice, *J. Photochem. Photobiol. B*, 2012, **107**, 14-19.

9 J. Harasym and R. Oledzki, *Nutrition*, 2014, **30**, 511-517.

10 G. N. Bosio, T. Breitenbach, J. Parisi, M. Reigosa, F. H. Blaikie, B. W. Pedersen, E. F. F. Silva, D. O. Mártire and P. R. Ogilby, *J. Am. Chem. Soc.*, 2013, **135**, 272-279.

11 G. Agati, E. Azzarello, S. Pollastri and M. Tattini, *Plant Science*, 2012, **196**, 67-76.

12 M. Montenegro, M. Nazareno, C. Borsarelli, *J. Photochem. Photobiol. A*, 2007, **186**, 47-56.

13 K. Mukai, S. Nagai and, K. Ohara, *Free Rad. Biol. Med.*, 2005, **39**, 752-761.

14 S. Nagai, K. Ohara and K. Mukai, *J. Phys. Chem. B.*, 2005, 109, 4234-4240.

15 N. K. Sahu, S. S. Balbhadra, J. Choudhary and D. V. Kohli, *Curr. Med. Chem.*, 2012, **19**, 209-225.

16 P. B. Babasaheb, A. P. Sachin, N. G Rajesh, L. K. Balaji, S. H. Balwant, N. K. Santosh and S. J. Shivkumar, *Bioorg. Med. Chem. Lett.*, 2010, **20**, 730-733.

17 S. Vogel, M. Barbic, G. Jürgenliemk and J. Heilmann, *Eur. J. Med. Chem.*, 2010, **45**, 2206-2213.

18 C. S. Chidan, W. S. Loh, C. W. Ooi, C. K. Quah and H. K. Fun, *Molecules*, 2013, **18**, 11996-12011.

19 J. Hyun and M. Yhung, *J. Food Sci.*, 2010, **75**, 506-513.

20 A. D. Becke, *J. Chem. Phys.*, 1993, **98**, 5648.

21 P. A. M. Dirac, *Proc. R. Soc. London, Ser. A.*, **1929**, 123, 714–733.

22 A. Schäfer, C. Huber and R. Ahlrichs, *J. Chem. Phys.*, 1994, **100**, 5829.

23 TURBOMOLE V6.3 2011, a development of University of Karlsruhe and Forschungszentrum Karlsruhe GmbH, 1989-2007, TURBOMOLE GmbH, since 2007; available from http://www.turbomole.com.

24 F. Furche and Ahlrichs, R., *J. Chem. Phys.,* 2002, **117**, 7433.

25 S. Grimme, J. Antony, S. Ehrlich and H. Krieg, *J. Chem. Phys*., 2010, **132**, 154104.

26 C. Reichardt, in Solvents and Solvent Effects in Organic Chemistry, Wiley-VCH, Weinheim, 1990.

27 A. Klamt and G. Schürmann, *J. Chem. Soc., Perkin Trans. 2*, 1993, 799.

28 A. Schäfer, A. Klamt, D. Sattel, J. C. W. Lohrenz and F. Eckert*, Phys. Chem. Chem. Phys*., 2000, **2**, 2187.

29 C. Kind, M. Reiher, and J. Neugebauer, SNF Version 2.2.1: A Program Package for Numerical Frequency Analyses; Universität Erlangen, 1999−2002.

30 S. Grimme and M. Waletzke, *J. Chem. Phys.*, 1999, **111**, 5645.

31 C. M. Marian and N. Gilka, *J. Chem. Theory Comput.,* 2008, **4**, 1501−1515.

32 M. R. Silva-Junior, M. Schreiber, S. P. A. Sauer and W. Thiel, *J. Chem. Phys.,* 2008, **128**, 104103.

33 A. Rodriguez-Serrano, M. C. Daza, M. Doerr and C. M. Marian, *Photochem. Photobiol. Sci.,* 2012, **11**, 397-408.

34 L. Claisen, A. Claparède, *Ber. Dtsch. Chem. Ges.*, 1881, **14**, 2460–2468; J. G. Schmidt, *Ber. Dtsch. Chem. Ges.*, 1881, **14**, 1459–1461; D. Pacheco, J. Trilleras, J. Quiroga, J. Gutiérrez, l. Prent, T. Coavas, J. Marín, G. Delgado, *J. Braz. Chem. Soc., 2013,* **24***,* 1685-1690.

35 P. Atkins, L. Jones, W.H. Freeman & Company (Ed.) Chemical Principles The Quest for Insight, New York, 2008, p. 556.

36 K. J. Jarag, D. V. Pinjari, A. B. Panditb and G. S. Shankarling, *Ultrason. Sonochem.*, 2011, **18**, 617-623.

37 K. Jadidi, R. Gharemanzadeh, M. Mehrdad, H. Darabi, H. Khavasi and D. Asgari, *Ultrason. Sonochem.,* 2008, **15**, 124-128.

38 R. Cella, H. Stefani, *Tetrahedron*, 2009, **65**, 2619-2641.

39 V. Calvino, M. Picallo, A. J. López-Peinado, R. M. Martín-Aranda and C. J. Durán-Valle, *Appl. Surf. Sci.*, 2006, **252**, 6071-6074.

40 P. B. Merkel and D. R. Kearns, *J. Am. Chem. Soc.*, 1972, **94**, 7244-7253.

41 M. J. Thomas and C. S. Foote, *Photochem. Photobiol*,. 1978, 27, 683-693.

42 I. Saito, T. Matsuura and K. Inoue, *J. Am. Chem. Soc.*, 1983, **105**, 3200-3206.

43 K. Inoue, T. Matsuura and I. Saito, *Tetrahedron*, 1985, **41**, 2177-2181.

44 A.P. Darmanyan, W. S. Jenks and P. Jardon, *J. Phys. Chem. A.*, 1998, **102**, 7420-7426.

45 F. M. Cabrerizo, M. L. Dántola, G. Petroselli, A. L. Capparelli, A. H. Thomas, A. M. Braun, C. Lorente and E. Oliveros, *Photochem. Photobiol.*, 2007, **83**, 526-534.

46 E. Lemp, N. Pizarro, M. V. Encinas and A. L. Zanocco, *Phys. Chem. Chem. Phys.*, 2001, **3**, 5222-5225.

47 M. Silva-Oliveira, M. Lima, D. Severino, M. da Silva-Baptista, P. Di Mascio and M. Tabak, *Photochem. Photobiol.*, 2007, **83**, 1379-1385.

48 S. Wang, G. Yu, J. Lu, K. Xiao, Y. Hu and H. Hu, *Synthesis*, 2003, 487-490.

49 J. I. Kim, J. H. Lee, D.S. Choi, B. M. Won, M. Y. Jung and J. Park, *J. Food Sci.*, 2009, **74**, 362-369.

50 K. Mukai, A. Ouchi and M. Nakano, *J. Agric. Food Chem.*, 2011, **59**, 1705-1712.

51 A. Ouchi, K. Aizawa, Y. Iwasaki, T. Inakuma, J. Terao, S. I. Nagaoka and M. Mukai, *J. Agric. Food Chem.*, 2010, **58**, 9967-9978.

52 A. F. Olea and F. Wilkinson, *J. Phys. Chem.*, 1995, **99**, 4518-4524.

53 **a)** J. Perdew, K. Burke and M. Ersernhof, *Phys. Rev. Lett.*, 1997, **78**, 1396. **b)** J. Janak, *Phys. Rev. B.* 1978, **1**8, 7175-7168.

54 R. G. Pearson, *J. Mol. Struct. (Theochem)*, 1992, **255**, 261-270.

55 R. G. Parr, L. Szentpaly and S. Liu, *J. Am. Chem. Soc.*, 1999, **121**, 1922-1924.

56 X. Zarate, E. Schott, T. Gomez, R. Arratia-Perez. *J. Phys. Chem. A*., 2013, **117**, 430−438.

57 P. K. Chattaraj and S. Giri, *Annu. Rep. Prog. Chem. Sect. C Phys. Chem.*, 2009, **105**, 13-39.

